LATTICE BOLTMANN SIMULATION OF FLOWS IN A LIQUID DROPLET ON A SOLID SURFACE WITH A HEAT FLUX

A.L. Kupershtokh & D.A. Medvedev*

Lavrentyev Institute of Hydrodynamics SB RAS, Novosibirsk, 630090, Russia

*Address all correspondence to: A.L. Kupershtokh, Lavrentyev Institute of Hydrodynamics SB RAS, Novosibirsk, 630090, Russia, E-mail: skn@hydro.nsc.ru

We study the flows arising in a liquid droplet placed on a heated solid surface. The flow arises due to simultaneous action of a nonuniform evaporation at the droplet surface and the Marangoni effect. Calculations are carried out with the lattice Boltzmann method taking into account the conductive and convective heat fluxes, the evaporation and the condensation, and the temperature dependence of the surface tension. We obtain the pictures of vortical liquid flow inside a droplet. We find that the contact angle can change due to the forces which arise during evaporation or condensation near the contact line. The influence of the droplet shape (which depends on the contact angle) on the possibility of the arising of vortical flows inside the droplet is shown.

KEY WORDS: *droplets, wettability, contact angle, heat transfer enhancement, vortical flow, heat flux, lattice Boltzmann method*

1. INTRODUCTION

Modern microfluidic and microelectronic devices require effective cooling of hot surfaces for their normal operation. Single-phase coolants achieved their limit of the heat flux, and now, cooling systems with the phase change are used, such as heat pipes. These devices are based on the heat absorption during the evaporation of liquid at the hot surfaces. One of the methods for cooling is the creation of thin films or many droplets of evaporating liquid placed onto a solid surface (Potash and Wayner, 1972; Wayner, 1989).

The heat flux from the surface increases significantly near the three-phase contact line that was measured in experiments (Ajaev and Kabov, 2017; Cheverda et al., 2017; Gibbons et al., 2016; Marchuk et al., 2015). This effect is important in the spray and film cooling of heated surfaces. Evaporation of a droplet placed onto a hot solid surface produces flows of liquid inside the droplet. These flows are caused by several reasons: the action of gravity, the nonuniform surface evaporation, and the Marangoni effect. In presence of heat fluxes from solid surface, the Marangoni effect becomes decisive for small droplets. The thermocapillary convection and heat fluxes inside droplets placed on a heated solid surface were investigated both experimentally and numerically (Albernaz et al., 2013; Alhendal and Touzani, 2023; Bartashevich et al., 2012; Chen et al., 2020; Deegan et al., 1997; Edwards et al., 2018; Gelderblom et al., 2022; Sui and Spelt, 2015). In calculations, however, the shape of a droplet was often assumed fixed.

In many problems with droplets, films or bubbles at a solid surface, the wetting of a surface plays an important role (de Gennes, 1985; de Gennes et al., 2004; Lalanne et al., 2021; Li et al., 2015; Moiseev et al., 2020); short review can be found in the work (Medvedev and Kupershtokh, 2022). The wetting determines the value of contact angles, and it depends on the properties both of the liquid and the surface. In the absence of other forces (electric, gas-dynamic, etc.) the value of the contact angle corresponds to the classic Young's law (Makkonen, 2016; Young, 1805). However, the intensive evaporation near the contact line creates forces along the solid surface and can influence on the value of the contact angle. This effect can be important, but it is practically not investigated.

Numerical simulation of the heat exchange processes near the contact line and the fluid flows in the evaporating or condensing droplets at a heated or cooled solid surface is a complicated task because of the presence of moving

Submitted: 9/18/25; Accepted: 12/2/25; Online: 12/3/25 https://doi.org/10.1615/InterfacPhenomHeatTransfer.2025061727
2169–2785/26/$35.00

NOMENCLATURE

A	free parameter in the forcing scheme
a	parameter in the van der Waals equation
B	wettability parameter
b	parameter in the van der Waals equation
Bo	Bond number
Bo_0	initial value of Bond number
$\mathbf{c}_k$	velocities of pseudoparticles
C_V	specific heat
E	internal energy of a unit volume
E_{ideal}	internal energy for ideal gas
E_{mol}	internal energy of one mole
$\mathbf{e}_k$	lattice vectors
$\mathbf{F}$	force acting on fluid
f_k	distribution functions for lattice Boltzmann method
f_k^{eq}	equilibrium distribution functions
G_k	weight coefficients
g	gravity acceleration
g_k	distribution functions for internal energy
g_k^{eq}	equilibrium distribution functions for internal energy
H	height of calculation region
h	height of droplet
L	width of calculation region
P	fluid pressure
Q	latent heat of evaporation
q	heat flux
R	gas constant
R_0	initial droplet radius
T	fluid temperature
U	pseudopotential
$\mathbf{u}$	fluid velocity
V	volume
w_j	weight coefficients for boundary conditions
w_k	weights in the equilibrium distribution functions

Greek Symbols

α	weight coefficient
γ	contact angle
ε	specific internal energy
λ	heat conductivity
ρ	fluid density
τ	relaxation time
τ_E	relaxation time for internal energy
Φ	function for force calculation
Ω_k	collision operator

Subscripts

L	liquid
V	vapor
x, y	spatial directions

phase boundaries at which the mass and energy fluxes should be adjusted correctly. Moreover, phase boundaries can appear, disappear and change their topology during the simulation. That requires engaging new computation methods. Recently, the lattice Boltzmann method (LBM) is more and more widely used to simulate flows of viscous liquids with phase transition between liquid and vapor. In this method, both phases are described uniformly, and the phase boundary is diffuse. The frequently used approach is based on the pseudopotential (Qian and Chen, 1997; see also Section 3). To simulate the convective and conductive heat transport, either finite-difference method (Li and Luo, 2014; Zhang and Chen, 2003) or the method of additional lattice Boltzmann component (Kupershtokh et al., 2014) are used.

In this work, we investigate numerically the behavior of a droplet placed at the solid surface using LBM with account for phase transition between liquid and vapor, convective and conductive heat transport, and action and temperature dependence of the surface tension. The surface is heated or cooled, which leads to either evaporation of liquid or condensation of vapor at the droplet surface. We obtain the liquid flow and the heat flux inside the droplet. Most of the numerical experiments are carried out for a neutrally wetting surface, and we observe the change of the value of contact angle comparing to the static one in cases of heated and cooled surface. We also make simulation with a wetting surface in order to elucidate the influence of wetting on the flows inside a droplet.

The structure of the paper is as follows. In Section 2, the lattice Boltzmann method is described briefly. In Section 3, the scheme to simulate phase transfer is presented. In Section 4, we describe how the heat transport is simulated. Section 5 is devoted to taking into account the latent heat of evaporation for the van der Waals equation of state. In Section 6, we discuss setting the initial and boundary conditions. Section 7 presents the simulation results. Some concluding remarks are given in Section 8.

2. LATTICE BOLTZMANN METHOD

LBM was firstly introduced in McNamara and Zanetti (1988). It is the solution of the discretized in space and time kinetic Boltzmann equation with a fixed finite set of pseudoparticle velocities determined by the lattice used (lattice vectors $\mathbf{e}_k = \mathbf{c}_k\Delta t$, $k = 0\ldots m$, Δt is the time step). The fluid is described by a set of one-particle distribution functions f_k. Their evolution equation for a time step Δt is given by

$$f_k(\mathbf{x} + \mathbf{c}_k\Delta t, t + \Delta t) = f_k(\mathbf{x}, t) + \Omega_k\{f_k\} + \Delta f_k. \tag{1}$$

Hydrodynamic variables (density ρ and mass velocity $\mathbf{u}$) are calculated as

$$\rho = \sum\nolimits_{k=0}^{m} f_k \quad \text{and} \quad \rho\mathbf{u} = \sum\nolimits_{k=1}^{m} \mathbf{c}_k f_k. \tag{2}$$

The simplest form of the collision operator is the relaxation to the local equilibrium with a single relaxation time (Bhatnagar–Gross–Krook model, BGK) (Bhatnagar et al., 1954; Qian et al., 1992):

$$\Omega_k\{f_k\} = (f_k^{eq}(\rho, \mathbf{u}) - f_k(\mathbf{x}, t))/\tau. \tag{3}$$

Nondimensional relaxation time τ determines the kinematic viscosity of a fluid $\nu = (\tau - 0.5)\theta\Delta t$. Here, θ is the normalized kinetic temperature of pseudoparticles, which is usually taken equal to $\theta = (\Delta x/\Delta t)^2/3$, where Δx is the lattice spacing. Equilibrium distribution functions are written in the form (Koelman, 1991)

$$f_k^{eq}(\rho, \mathbf{u}) = \rho w_k \left(1 + \frac{\mathbf{c}_k\mathbf{u}}{\theta} + \frac{(\mathbf{c}_k\mathbf{u})^2}{2\theta^2} - \frac{\mathbf{u}^2}{2\theta}\right). \tag{4}$$

Two-dimensional variant D2Q9 with nine pseudoparticle velocity vectors on a square lattice ($m = 8$) is used in calculations. Weight coefficients w_0, w_{1-4}, and w_{5-8} in this case are equal to 4/9, 1/9, and 1/36, correspondingly.

The exact difference method (EDM) (Kupershtokh, 2004, 2010) is used to take into account the change of distribution functions Δf_k under the action of internal and external body forces

$$\Delta f_k = f_k^{eq}(\rho, \mathbf{u} + \Delta\mathbf{u}) - f_k^{eq}(\rho, \mathbf{u}). \tag{5}$$

Here, the velocity change $\Delta\mathbf{u}$ in one time step is determined by the total force $\mathbf{F}$, acting on the fluid at a node, $\Delta\mathbf{u} = \mathbf{F}\Delta t/\rho$. The physical velocity $\mathbf{u}^*$ should be taken at the half-step according to the formula (Ginzburg and Adler, 1994)

$$\rho\mathbf{u}^* = \sum\nolimits_{k=1}^{m} \mathbf{c}_k f_k + \mathbf{F}\Delta t/2. \tag{6}$$

3. COMPUTER SIMULATION OF PHASE TRANSITIONS

LBM is an interface-capturing method. Instead of a density discontinuity, a thin transition layer liquid—vapor is simulated where the density varies continuously (the diffuse interface method). Liquid and gas phases are described uniformly. In order to achieve phase separation, forces are introduced acting on the fluid at a node from neighbor nodes (pseudopotential method) (Qian and Chen, 1997). The total force acting in a node has the form

$$\mathbf{F} = -\nabla U, \tag{7}$$

where pseudopotential $U = P(\rho, T) - \rho\theta$ is expressed through the equation of state. These forces also provide the surface tension at the phase boundary.

The special hybrid isotropic approximation of the pseudopotential gradient proposed in Kupershtokh (2005) and Kupershtokh et al. (2009) is used:

$$\mathbf{F}(\mathbf{x}) = \frac{1}{\alpha\Delta x}\left[A\sum_{k=1}^{b} G_k\Phi^2(\mathbf{x} + \mathbf{e}_k)\,\mathbf{e}_k + (1 - 2A)\Phi(\mathbf{x})\sum_{k=1}^{b} G_k\Phi(\mathbf{x} + \mathbf{e}_k)\,\mathbf{e}_k\right]. \tag{8}$$

Here, the function $\Phi(\mathbf{x}) = \sqrt{-U}$ is expressed through the equation of state for the fluid

$$\Phi(\mathbf{x}) = \sqrt{\rho\theta - P(\rho, T)}. \tag{9}$$

For the model D2Q9, the value of α is equal to 3/2.

4. HEAT TRANSPORT

The passive scalar method (Kupershtokh et al., 2014, 2018) is used to simulate the convective heat flux. Here, an additional set of distribution functions g_k is introduced with the evolution equation

$$g_k(\mathbf{x} + \mathbf{c}_k\Delta t, t + \Delta t) = g_k(\mathbf{x}, t) + \frac{g_k^{eq}(\rho, \mathbf{u}(\mathbf{x}, t)) - g_k(\mathbf{x}, t)}{\tau_E} + \Delta g_k(\mathbf{x}, t). \tag{10}$$

Here, τ_E is the nondimensional relaxation time. The internal energy of a unit volume is calculated as

$$E = \sum\nolimits_{k=0}^{m} g_k. \tag{11}$$

Equilibrium distribution functions $g_k^{eq}(E, \mathbf{u})$ are similar to those given by Eq. (4). The work of pressure is equal to $-P\mathrm{div}\,\mathbf{u}$. The conductive heat flux is determined by the Fourier law $\mathbf{q} = -\lambda\,\nabla T$, where λ is the thermal conductivity. The change of the internal energy due to the work of pressure and the conductive heat flux is equal to

$$\frac{dE}{dt} = -P\mathrm{div}\,\mathbf{u}^* - \mathrm{div}\,\mathbf{q}. \tag{12}$$

It is calculated using usual finite-difference method.

Corresponding changes in the distribution functions per time step are equal to

$$\Delta g_k^{(1)}(\mathbf{x}, t) = g_k(\mathbf{x}, t)\frac{1}{E}\frac{dE}{dt}\Delta t. \tag{13}$$

In order to prevent the parasitic spread of the internal energy at phase boundaries, special "pseudoforces" for the energy scalar are introduced (Kupershtokh et al., 2014, 2018) similar to Eq. (5)

$$\Delta g_k^{(2)}(\mathbf{x}, t) = g_k^{eq}(E, \mathbf{u} + \Delta\mathbf{u}) - g_k^{eq}(E, \mathbf{u}). \tag{14}$$

The total change of distribution functions in Eq. (8) is equal to $\Delta g_k = \Delta g_k^{(1)} + \Delta g_k^{(2)}$.

There is a diffusion of internal energy in LBM related to the relaxation time τ_E. Hence, the effective diffusion coefficient is the sum $\lambda_{\text{eff}} = \lambda + \rho C_V(\tau_E - 0.5)\theta\Delta t$. Here, C_V is the specific heat at constant volume of the fluid. For $\tau_E \to 0.5$ the second term can be neglected.

This scheme was validated in Kupershtokh et al. (2023) for the case of a uniform fluid flow between two surfaces with fixed temperatures. In this case, the analytical solution exists. The temperatures of left and right surfaces are T_0 and $T_L = T_0 - \Delta T$. The flow velocity u, the specific heat C_V, the fluid density ρ, and the heat conductivity λ are constant. The solution for the coordinate dependence of the fluid temperature is

$$T(x) = T_0 - \Delta T\frac{\exp(\rho C_V u x/\lambda) - 1}{\exp(\rho C_V u L/\lambda) - 1}. \tag{15}$$

Here, L is the distance between surfaces. The Péclet number is $\mathrm{Pe} = \rho C_V u L/\lambda$. Results of the calculations are in very good agreement with theoretical ones both in the case of small and large Péclet number.

5. LATENT HEAT OF PHASE TRANSITION FOR VAN DER WAALS EQUATION OF STATE

Internal energy of one mole of fluid is expressed by the formula $E_{\text{mol}} = E_{\text{ideal}} - a/V$ for the van der Waals equation of state

$$P = \frac{RT}{V-b} - \frac{a}{V^2}. \tag{16}$$

For a unit mass this gives $\varepsilon = C_V T - a\rho$ (specific internal energy). The latent heat of phase transition Q is the change of internal energy of the fluid in the process of density decrease from the density of liquid ρ_L to the one of vapor ρ_V at constant temperature. From the expression for internal energy, one obtains

$$Q = \varepsilon_V - \varepsilon_L = -a(\rho_V - \rho_L). \tag{17}$$

Here, ρ_L and ρ_V are the equilibrium density of liquid and vapor. The temperature dependence of the latent heat $Q(T)$ is taken into account implicitly through the temperature dependence of ρ_L and ρ_V. The evaporation heat decreases to zero as the temperature approaches the critical value.

Thus, we obtain for the change of the internal energy in a cell of the transition layer liquid–vapor due to the phase transition

$$\frac{dE}{dt} = \frac{\rho_L Q(T)}{\rho_L - \rho_V}\frac{d\rho}{dt}. \tag{18}$$

It is assumed that the latent heat of phase transition Q is released or absorbed in the range of density $[\rho_V, \rho_L]$. Then, taken into account Eq. (17), one obtains

$$\frac{dE}{dt} = a\rho_L \frac{d\rho}{dt} = -a\rho_L\, \rho\, \mathrm{div}(\mathbf{u}^*). \tag{19}$$

6. INITIAL AND BOUNDARY CONDITIONS

The calculations are performed in a two-dimensional region $L \times H$ (Fig. 1). Initially, the temperature is constant $T_0 = 0.7$, and the velocity u is equal to zero everywhere (here and below, the temperature is nondimensionlized by the critical value T_{cr}). Then the temperature of the lower substrate is increased to the value $T(x,0) = T_0 + \Delta T$, and the temperature at the upper boundary is decreased to $T(x,H) < T_0$. In the case of the absence of vertical walls, the periodic boundary conditions for distribution functions and temperature along the x coordinate can be used: $f_k(L,y) = f_k(0,y)$, $g_k(L,y) = g_k(0,y)$, and $T(L,y) = T(0,y)$. No-flow and no-slip boundary conditions are used at solid walls, which is simulated in the LBM by the "bounce-back" rule for distribution functions. For the internal energy, equilibrium values are used corresponding to the surface temperature and to the density in the nearest liquid node.

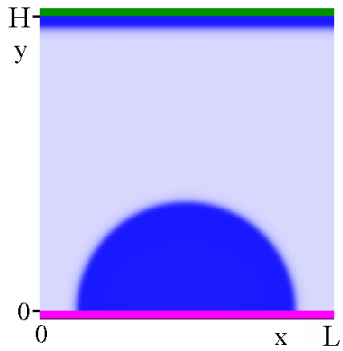

FIG. 1: Droplet of hemispherical shape on the neutrally wetted surface (γ = 90°) before the switch-on of heating. Initial droplet radius is $R_0 = 0.375H$. Grid size 200 × 200, $t = 0$.

For simulating the surface wetting in the LBM, the approaches are commonly used where interaction forces are introduced between the liquid or vapor in a node and n-nearest solid nodes. The method of simple attraction forces (Benzi et al., 2006; Kupershtokh and Medvedev, 2024) has the form

$$\mathbf{F}(\mathbf{x}) = \Phi(\mathbf{x}) \sum_{j=1}^{n} w(\mathbf{e}_j) B \Phi_{\text{solid}}(\mathbf{x} + \mathbf{e}_j) \cdot \mathbf{e}_j. \tag{20}$$

The values of Φ_{solid} in the boundary nodes are set equal to the values of $\Phi(\mathbf{x})$ in the neighbor liquid nodes. The parameter B (the adhesion parameter) determines the surface wetting and the contact angle. The value of $B = 1$ corresponds to the neutral wetting (contact angle $\gamma_0 = 90°$, Fig. 1). Larger values of B produce smaller contact angles, and vice versa. In the absence of other forces (electric, gas-dynamic, etc.) the value of the contact angle corresponds to the classic Young's law (Makkonen, 2016; Young, 1805).

7. DROPLETS ON A SOLID SURFACE: SIMULATION RESULTS

We simulate a droplet on the solid surface without the gravity field. Wettability of the surface is set such that without heat fluxes it is neutral ($B = 1$). For calculations presented in Figs. 2–8, the surface temperature is set equal to $T(x, 0) = 0.75$, and the temperature of the upper boundary decreases to $T(x, H) = 0.6$. The pictures are obtained of flows inside the droplet placed on the heated surface. These flows are produced by the action of a nonuniform evaporation at the droplet surface, and the Marangoni effect.

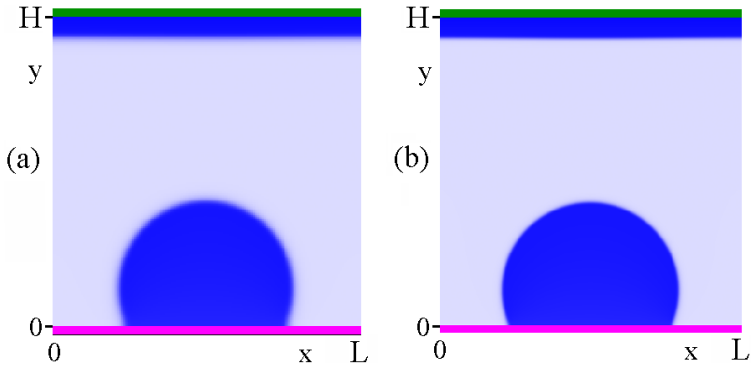

FIG. 2: Droplet shape after the switch-on of heating. Grid sizes 200 × 200 (a) and 400 × 400 (b), $t = 25{,}000$.

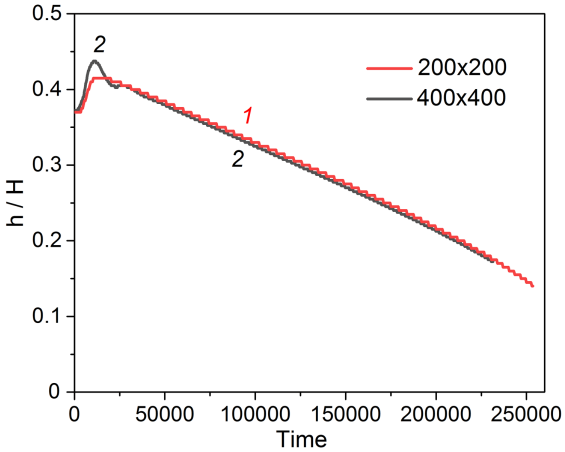

FIG. 3: Relative droplet height h/H vs. time for the calculations on grids 200 × 200 (curve *1*) and 400 × 400 (curve *2*)

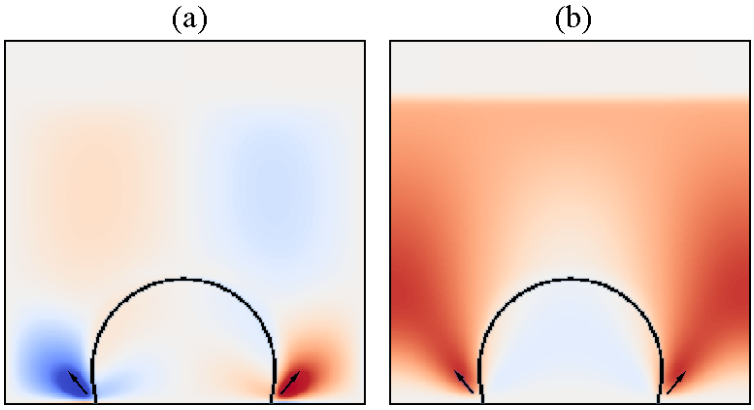

FIG. 4: Distribution of the horizontal u_x (a) and vertical u_y (b) fluid velocity for the evaporating droplet. Grid size 200 $\times$ 200, t = 25,000.

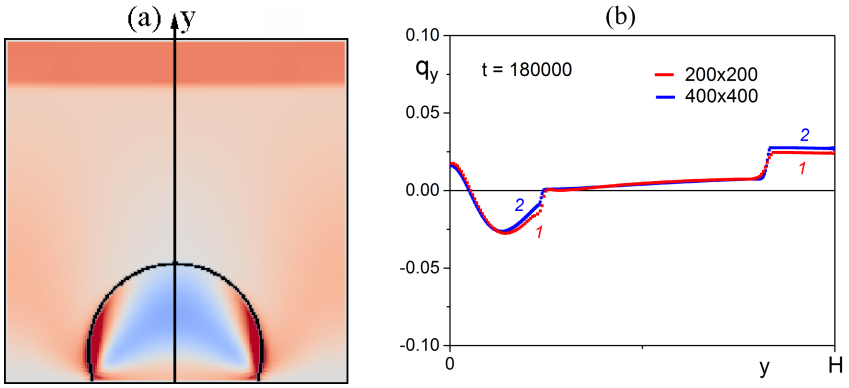

FIG. 5: (a) Vertical component of the heat flux q_y for the evaporating droplet (grid size 200 $\times$ 200, t = 25,000). (b) Heat flux vs. coordinate y along the droplet axis. Grid sizes 200 $\times$ 200 (curve *1*) and 400 $\times$ 400 (curve *2*), t = 180,000.

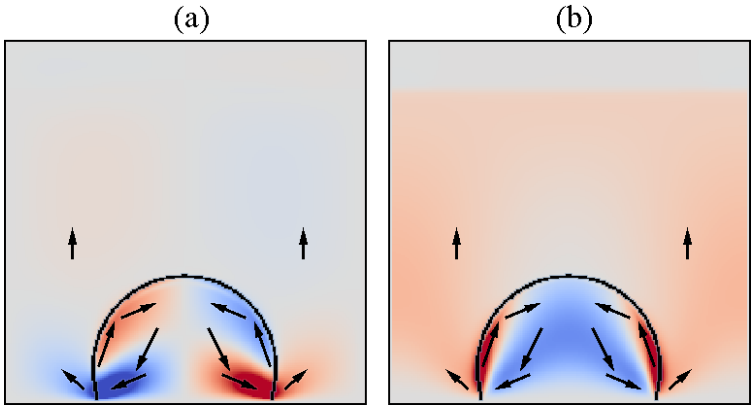

FIG. 6: Distribution of the fluid mass fluxes: horizontal $j_x = \rho u_x$ (a) and vertical $j_y = \rho u_y$ (b). Grid size 200 $\times$ 200, t = 25,000.

In order to validate the LBM method, the calculations are carried out on the grids 200 $\times$ 200 [Fig. 2(a)] and 400 $\times$ 400 [Fig. 2(b)]. Calculation parameters are adjusted to provide the same initial values of the dimensionless Bond number $\mathrm{Bo}_0 = \rho_L g R_0^2/\sigma$, which indicates the importance of gravitational forces compared to surface tension forces.

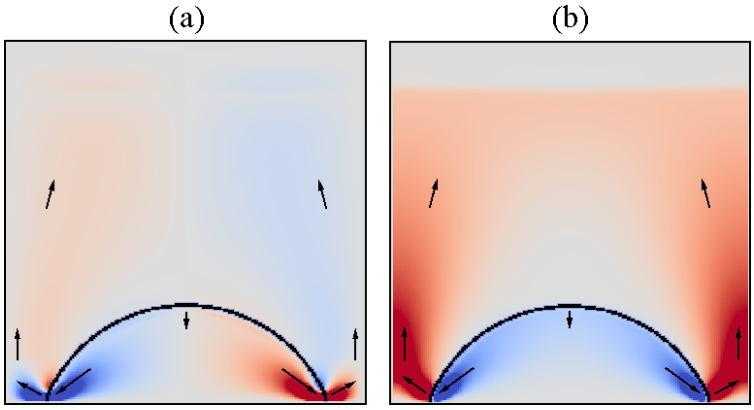

FIG. 7: Distribution of the horizontal j_x (a) and vertical j_y mass flux (b) inside the droplet on a wetting surface. Grid size 200 $\times$ 200, t = 15,000.

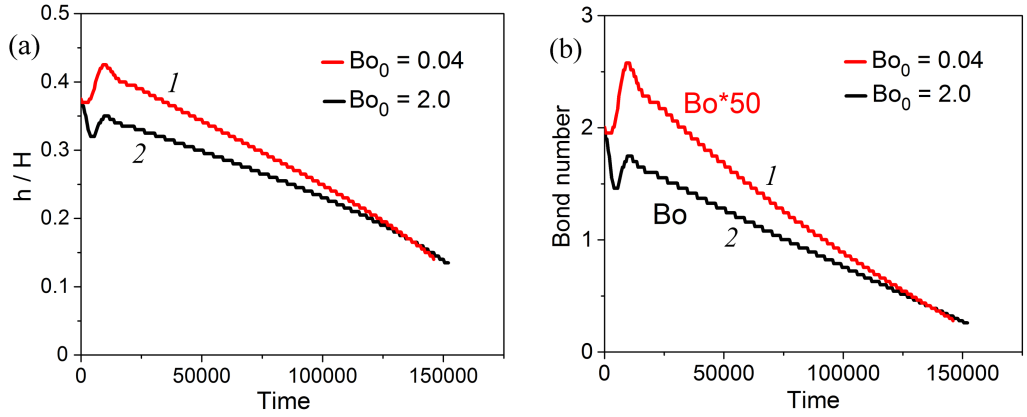

FIG. 8: (a) Time dependence of the relative droplet height h/H for different values of the gravity field, corresponding to the initial values of the Bond number $\mathrm{Bo}_0 = 0.04$ (curve *1*) and 2.0 (curve *2*). (b) Time dependence of the Bond number for different values of the gravity field.

Here, g is the gravity acceleration and σ is the coefficient of surface tension. In both simulations, the initial values are equal to $\mathrm{Bo}_0 = 0.04$. Hence, the shape of the droplets is the same in both cases. Note that the contact angle observed for evaporating droplet (Fig. 2) is greater than the value of static angle, despite the fact that it is essentially a receding contact angle. Hence, this effect cannot be explained by the well-known contact angle hysteresis (Eral et al., 2013).

Moreover, the comparison of the relative droplet height h/H in these calculations shows very good agreement (Fig. 3). Here, h is the current height of the droplet. The values of nondimensional time are presented for the variant with the grid 200 $\times$ 200. For the grid 400 $\times$ 400, the time step is twice smaller; hence, the same time value means the doubled number of iterations.

The intense evaporation of liquid near the contact line leads to some increase in the contact angle (see Figs. 1 and 2). Two factors determine this increase: the evaporation from the phase boundary itself, and the mechanical reaction forces similar to the Leidenfrost effect (Ajaev and Kabov, 2021; Kabov et al., 2016; Leidenfrost, 1966).

Figure 4 presents the distribution of fluid velocity at the 2D simulations of the evaporation of a droplet placed on the horizontal surface with neutral wetting. In all figures, the positively directed velocity is shown by red, and negatively directed one by blue. An intense evaporation of liquid is observed near the contact line [Fig. 4(a)]. A condensation of vapor occurs at the colder upper boundary.

The vertical component of the heat flux is shown in Fig. 5. The energy flux consists of the conductive part and the convective part associated with the mass flux. The conductive flux $q_y = -\lambda\,\partial T/\partial y$ prevails in the thin layer inside

the droplet near the lower boundary. In the central part of the droplet, the heat flux is directed downwards with the corresponding fluid flow [Figs. 5(b) and 6]. In the liquid film adjacent to the upper boundary, the heat flux is higher than the one in gas due to the energy release at the phase boundary due to the condensation of vapor.

The surface tension changes with height along the droplet boundary. In this case, it is lower near the heated boundary. Thus, toroidal axisymmetric vortices are produced in the droplet placed on the heated surface by the Marangoni surface forces (Fig. 6). The flow in these vortices is directed downwards near the axis of the droplet, and upwards near its surface.

The influence of the droplet shape is shown on the possibility of vortical flows inside the droplet. The shape depends on the surface wetting. When the wettability of the heated surface increases (contact angle $\gamma_0 = 75^\circ$), the vortical structures inside the droplet may not arise (Fig. 7), because the shape of the droplet with the same volume becomes flatter comparing with the case of neutral wettability ($\gamma_0 = 90^\circ$, Fig. 6).

The influence of the gravity field on the droplet behavior is shown in Fig. 8. Curves *1* and *2* correspond to initial values of the Bond number $\mathrm{Bo}_0 = 0.04$ and 2.0. When the initial value of Bond number is large enough, the height of the droplet begins to decrease at the initial stage [Fig. 8(a), curve *2*], and the droplet becomes flatter. For small initial value of Bond number, the height of the droplet h begins to increase at the initial stage [Fig. 8(a), curve *1*] due to the increase in the contact angle, as it was demonstrated above. It is possible to introduce the current Bond number $\mathrm{Bo} = \rho_L g h^2/\sigma$ for the droplet shape close to the hemispherical one. The current Bond number decreases when the droplet evaporates [Fig. 8(b)].

If, on the contrary, the lower boundary is cooled down to $T(x,0) = 0.65$, and the temperature of the upper boundary is $T(x,H) = 0.75$, the surface tension increases when approaching the colder surface. In this case, the direction of flows inside the droplet is the opposite to the previous case in accordance with the Marangoni effect. Hence, the toroidal axisymmetric vortices appear (Fig. 9), where the flow is directed upwards near the axis of the droplet, and downwards near its surface. The condensation of vapor proceeds in the vicinity of the contact line. This leads to some decrease in the contact angle relative to the equilibrium neutral one.

8. CONCLUSIONS

We use the lattice Boltzmann method to study the flows arising in a liquid droplet placed on a solid surface for small and moderate values of the Bond number. Phase transition between liquid and vapor, convective and conductive heat transport, and surface tension are taken into account. The flows are caused by the Marangoni effect and by the nonuniform evaporation and condensation on the droplet surface. A toroidal vortex is generated inside the droplet placed on the heated surface. In this case, a downward flow along the axis is produced. The heat flux inside the droplet is mostly directed along the flow, except the part adjacent to the solid surface, where the flow velocity is small, and the conductive heat flux prevails. Due to an intense evaporation near the contact line, there is some increase in the contact angle comparing to the equilibrium value for neutral wetting. It is shown that the contact angle observed for evaporating droplet is greater than the value of static angle, despite the fact that it is essentially a receding contact angle. Similarly, in the case of a droplet on the cooled surface, the contact angle decreases comparing with the static value, and despite it is essentially an advancing one. Hence, this effect cannot be explained by the well-known contact angle hysteresis. When the surface is cooled, the vortex rotates in an opposite direction. The direction of the heat flux

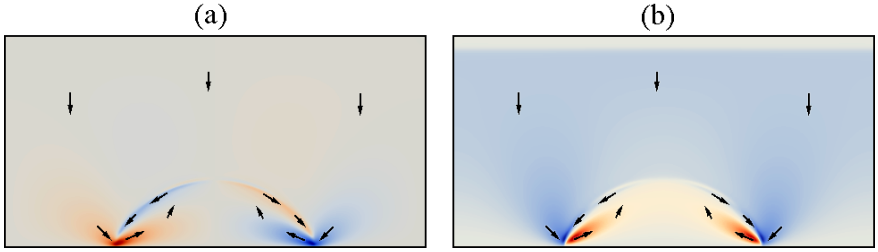

FIG. 9: Distribution of the fluid mass fluxes: horizontal $j_x = \rho u_x$ (a) and vertical $j_y = \rho u_y$ (b) in the case of the cooled lower surface. The total heat flux is directed downwards. Grid size 400×200, $t = 40{,}000$.

is also reverted. If the wettability is higher, the droplet shape becomes flatter, and vortical flows may not develop. With increasing the Bond number by a factor of 50, the initial shape of the droplet changes. The droplet becomes flatter for the larger value of gravity. This influences the evolution of the droplet height at the initial stage. During the evaporation, the droplet becomes smaller, the current Bond number decreases, and the graphs of the height get close.

ACKNOWLEDGMENT

The work is supported by the grant of Russian Science Foundation No. 25-29-00310, https://rscf.ru/project/25-29-00310/.

REFERENCES

Ajaev, V.S. and Kabov, O.A., Heat and Mass Transfer near Contact Lines on Heated Surfaces, *Int. J. Heat. Mass Transf.*, vol. **108**, Part A., pp. 918–932, 2017.

Ajaev, V.S. and Kabov, O.A., Levitation and Self-Organization of Droplets, *Ann. Rev. Fluid Mech.*, vol. **53**, pp. 203–225, 2021.

Albernaz, D.L., Do-Quang, M., and Amberg, G., Lattice Boltzmann Method for the Evaporation of a Suspended Droplet, *Interf. Phenom. Heat Transf.*, vol. **1**, no. 3, pp. 245–258, 2013.

Alhendal, Y. and Touzani, S., Effects of Sidewall Heat Flux on Thermocapillary Droplet Migration, *Interf. Phenom. Heat Transf.*, vol. **11**, no. 3, pp. 71–85, 2023.

Bartashevich, M.V., Marchuk, I.V., and Kabov, O.A., Numerical Simulation of Natural Convection in a Sessile Liquid Droplet, *Thermophys. Aeromech.*, vol. **19**, no. 2, pp. 317–328, 2012.

Benzi, R., Biferale, L., Sbragaglia, M., Succi, S., and Toschi, F., Mesoscopic Modeling of a Two-Phase Flow in the Presence of Boundaries: The Contact Angle, *Phys. Rev. E*, vol. **74**, no. 1, p. 021509, 2006.

Bhatnagar, P.L., Gross, E.P., and Krook, M.K., A Model for Collision Process in Gases. I. Small Amplitude Process in Charged and Neutral One-Component System, *Phys. Rev.*, vol. **94**, no. 3, pp. 511–525, 1954.

Chen, Y., Hong, F., and Cheng, P., Transient Flow Patterns in an Evaporating Sessile Drop: A Numerical Study on the Effect of Volatility and Contact Angle, *Int. Commun. Heat. Mass Transf.*, vol. **112**, p. 104493, 2020.

Cheverda, V.V., Karchevsky, A.L., Marchuk, I.V., and Kabov, O.A., Heat Flux Density in the Region of Droplet Contact Line on a Horizontal Surface of a Thin Heated Foil, *Thermophys. Aeromech.*, vol. **24**, no. 5, pp. 803–806, 2017.

Deegan, R.D., Bakajin, O., Dupont, T.F., Huber, G., Nagel, S.R., and Witten, T.A., Capillary Flow as the Cause of Ring Stains from Dried Liquid Drops, *Nature*, vol. **389**, pp. 827–829, 1997.

de Gennes, P.G., Wetting: Statics and Dynamics, *Rev. Mod. Phys.*, vol. **57**, no. 3, p. 827, 1985.

de Gennes, P.G., Brochard-Wyart, F., and Quéré, D., *Capillarity and Wetting Phenomena: Drops, Bubbles, Pearls, Waves*, New York: Springer, 2004.

Edwards, A.M.J., Atkinson, P.S., Cheung, C.S., Liang, H., Fairhurst, D.J., and Ouali, F.F., Density-Driven Flows in Evaporating Binary Liquid Droplets, *Phys. Rev. Lett.*, vol. **121**, no. 18, p. 184501, 2018.

Eral, H.B., 't Mannetje, D.J.C.M., and Oh, J.M., Contact Angle Hysteresis: A Review of Fundamentals and Applications, *Colloid. Polym. Sci.*, vol. **291**, no. 2, pp. 247–260, 2013.

Gelderblom, H., Diddens, C., and Marin, A., Evaporation-Driven Liquid Flow in Sessile Droplets, *Soft Matter*, vol. **18**, pp. 8535–8553, 2022.

Gibbons, M.J., Howe, C.M., Di Marco, P., and Robinson, A.J., Local Heat Transfer to an Evaporating Sessile Droplet in an Electric Field, *J. Phys. Conf. Ser.*, vol. **745**, no. 3, p. 032066, 2016.

Ginzburg, I. and Adler, P.M., Boundary Flow Condition Analysis for the Three-Dimensional Lattice Boltzmann Model, *J. Phys. II France*, vol. **4**, no. 2, pp. 191–214, 1994.

Kabov, O.A., Zaitsev, D.V., Kirichenko, D.P., and Ajaev, V.S., Investigation of Moist Air Flow near Contact Line Using Micro-droplets as Tracers, *Interf. Phenom. Heat Transf.*, vol. **4**, nos. 2-3, pp. 207–216, 2016.

Koelman, J.M.V.A., A Simple Lattice Boltzmann Scheme for Navier–Stokes Fluid Flow, *Europhys. Lett.*, vol. **15**, no. 6, pp. 603–607, 1991.

Kupershtokh, A.L., New Method of Incorporating a Body Force Term into the Lattice Boltzmann Equation, in *Proc. 5th Int. EHD Workshop*, Poitiers, France, pp. 241–246, 2004.

Kupershtokh, A.L., Simulation of Flows with Liquid–Vapor Interfaces by the Lattice Boltzmann Method, *Vestnik NGU (Quarterly J. Novosibirsk State Univ.), Ser.: Math. Mech. Inform.*, vol. **5**, no. 3, pp. 29–42, 2005. (in Russian)

Kupershtokh, A.L., Medvedev, D.A., and Karpov, D.I., On Equations of State in a Lattice Boltzmann Method, *Comput. Math. Appl.*, vol. **58**, no. 5, pp. 965–974, 2009.

Kupershtokh, A.L., Criterion of Numerical Instability of Liquid State in LBE Simulations, *Comput. Math. Appl.*, vol. **59**, no. 7, pp. 2236–2245, 2010.

Kupershtokh, A.L., Medvedev, D.A., and Gribanov, I.I., Modeling of Thermal Flows in a Medium with Phase Transitions Using the Lattice Boltzmann Method, *Numer. Methods Prog.*, vol. **15**, no. 2, pp. 317–328, 2014. (in Russian)

Kupershtokh, A.L., Medvedev, D.A., and Gribanov, I.I., Thermal Lattice Boltzmann Method for Multiphase Flows, *Phys. Rev. E*, vol. **98**, no. 2, p. 023308, 2018.

Kupershtokh, A.L., Medvedev, D.A., and Alyanov, A.V., Simulation of Substrate Cooling during Evaporation of Pure Vapor from the Surface of a Thin Film and Liquid Drops, *J. Appl. Ind. Math.*, vol. **17**, no. 3, pp. 582–591, 2023.

Kupershtokh, A.L. and Medvedev, D.A., On Contact Wetting Angles in the Lattice Boltzmann Method and Their Measurement, *Eurasian J. Math. Comp. Appl.*, vol. **12**, no. 4, pp. 84–91, 2024.

Lalanne, C., Magdelaine, Q., Lequien, F., and Fullana, J.-M., Numerical Model Using a Volume-of-Fluid Method for the Study of Evaporating Sessile Droplets in Both Unpinned and Pinned Modes, *Eur. J. Mech. B Fluids*, vol. **89**, pp. 267–273, 2021.

Leidenfrost, J.G., A Tract about Some Qualities of Common Water (1756), *Int. J. Heat Mass Transf.*, vol. **9**, no. 11, pp. 1153–1166, 1966.

Li, Q. and Luo, K.H., Effect of the Forcing Term in the Pseudopotential Lattice Boltzmann Modeling of Thermal Flows, *Phys. Rev. E*, vol. **89**, no. 5, p. 053022, 2014.

Li, Q., Luo, K.H., Kang, D.Q., and Chen, Q., Contact Angles in the Pseudopotential Lattice Boltzmann Modeling of Wetting, *Phys. Rev. E*, vol. **90**, no. 5, p. 053022, 2015.

Makkonen, L., Young's Equation Revisited, *J. Phys.: Condens. Matter*, vol. **28**, no. 13, p. 135001, 2016.

Marchuk, I., Karchevsky, A., Surtaev, A., and Kabov, O., Heat Flux at the Surface of Metal Foil Heater under Evaporating Sessile Droplets, *Int. J. Aerospace Eng.*, vol. **2015**, p. 391036, 2015.

McNamara, G.R. and Zanetti, G., Use of the Boltzmann Equation to Simulate Lattice-Gas Automata, *Phys. Rev. Lett.*, vol. **61**, no. 20, pp. 2332–2335, 1988.

Medvedev, D.A. and Kupershtokh, A.L., Liquid Dielectric Films in a Nonuniform Electric Field: Dynamics, Perforation, and Influence of Electrode Wettability, *Interf. Phenom. Heat Transf.*, vol. **10**, no. 2, pp. 41–51, 2022.

Moiseev, M.I., Fedoseev, A.V., Shugaev, M., and Surtaev, A.S., Hybrid Thermal Lattice Boltzmann Model for Boiling Heat Transfer on Surfaces with Different Wettability, *Interf. Phenom. Heat Transf.*, vol. **8**, no. 1, pp. 81–91, 2020.

Potash, M. and Wayner, P.C., Evaporation from a Two-Dimensional Extended Meniscus, *Int. J. Heat Mass Transf.*, vol. **15**, no. 10, pp. 1851–1863, 1972.

Qian, Y.H., d'Humiéres, D., and Lallemand, P., Lattice BGK Models for Navier–Stokes Equation, *Europhys. Lett.*, vol. **17**, no. 6, pp. 479–484, 1992.

Qian, Y.-H. and Chen, S., Finite Size Effect in Lattice-BGK Models, *Int. J. Mod. Phys. C*, vol. **8**, no. 4, pp. 763–771, 1997.

Sui, Y. and Spelt, P.D.M., Non-Isothermal Droplet Spreading/Dewetting and Its Reversal, *J. Fluid Mech.*, vol. **776**, pp. 74–95, 2015.

Wayner, P.C., A Dimensionless Number for the Contact Line Evaporative Heat Sink, *J. Heat Transf.*, vol. **111**, no. 3, pp. 813–815, 1989.

Young, T., III. An Essay on the Cohesion of Fluids, *Philos. Trans. R. Soc.*, vol. **95**, no. 3, pp. 65–87, 1805.

Zhang, R. and Chen, H., Lattice Boltzmann Method for Simulations of Liquid-Vapor Thermal Flows, *Phys. Rev. E*, vol. **67**, no. 6, p. 066711, 2003.